A New Blind Adaptive Beamformer for Underwater Communications

H. S. Hung, H. Y. Hsiao and Y. L. Chien

Department of Electrical Engineering
National Taiwan Ocean University
2 Pei-Ning Rd, Keelung, Taiwan
Email: b0221@mail.ntou.edu.tw

***Abstract*-In this paper, a new blind adaptive beamformer is proposed for underwater communications. It exploits the cyclostationary property of modulated communication signals, which arises from carrier frequencies or baud rates. Spectral lines are generated by processing the underlying QPSK modulated signal via down-conversion, conjugation and multiplication. The beamformer coefficients are determined by minimizing the mean square error between the processed signal with spectral lines and a complex exponential extracted by phase-locked loop. Compared to traditional adaptive beamformers, the proposed beamformer is robust against the pointing error of the desired signal and the positioning error of the hydrophone array.**

To overcome the intersymbol interference, a decision feedback equalizer is combined with the proposed beamformer. Simulation results show that the proposed space-time processor is very effective for various channel models.

I. INTRODUCTION

In underwater communications, beamformer is mainly used at the first stage in a receiver as a spatial filter. It processes the received signal from an array of hydrophones to point its main beam toward the direction of the desired signal whereas the nulls of its side lobes toward the interference signals. This results in an improvement of signal-to-noise plus interference ratio. Traditional beamformers, such as delay-sum (DS) and minimum variance distortionless response (MVDR) beamformers, require to know the incident angle of the desired signal and are also very sensitive to its pointing error as well as the positioning error of the sensor array [1]. To overcome the drawbacks of traditional beamformers, a blind adaptive beamformer was proposed by Casterdo [2], which exploits cyclostationary property often found in communication signals. It has relatively simple structure and yet better performance than other methods, such as SCORE [3] and constant modulus (CM) [4]. Inspired by Casterdo's approach, in this paper we propose a new blind adaptive beamformer (BAB) which differs from [2] in the ways of extracting the reference signal (complex exponential) and the signal that generates a dominant spectral line at the same frequency as the reference signal. In [5], p-power nonlinearity in conjunction with the extended Kalman filter is used. Although p-power processing is conceptually simple, it suffers the drawback of higher sampling rate when p is large. Higher sampling rate will increase the cost of analog-to-digital converter and also make real-time processing more difficult.

To overcome the problems of directional interference and intersymbol interference (ISI), a space-time processor is proposed. This processor incorporates the new BAB with a decision feedback equalizer (DFE). Computer simulations are performed to show the effectiveness of the proposed space-time processor under various types of channel model.

II. SPECTRAL LINE GENERATION

In this paper, we adopt quadrature phase shift keying (QPSK) as the modulation scheme, which can be represented as

$$y(t) = [I(t) + jQ(t)]e^{j2\pi f_c t+\phi} \tag{2.1}$$

where $I(t)$ and $Q(t)$ are the in-phase and quadrature components of baseband signal respectively, f_c denotes the carrier frequency, and ϕ is the phase error between the local oscillator and the transmitted carrier. Let $d(t)$ be the complex exponential $e^{j2\pi f_c t}$ which can be obtained by a phase-locked loop (PLL). If the bandpass signal $y(t)$ is first down converted in frequency to the baseband $z(t)$ as

$$z(t) = y(t)d^*(t) = [I(t) + jQ(t)]e^{j\phi} \tag{2.2}$$

Then by taking the complex conjugate of $z(t)$ and multiplying it with $y(t)$, we have

$$L(t) = y(t)z^*(t) = [I^2(t) + Q^2(t)]e^{j2\pi f_c t} \tag{2.3}$$

Fig.1 shows the power spectrum of $L(t)$ which contains one dominant peak at f_c = 0.25 and the other two peaks at $f_c \pm r$, where r is the symbol rate. It is evident that line spectra of QPSK signal can be obtained by <u>d</u>own-frequency conversion, <u>c</u>onjugation and <u>m</u>ultiplication and this process will be called DCM.

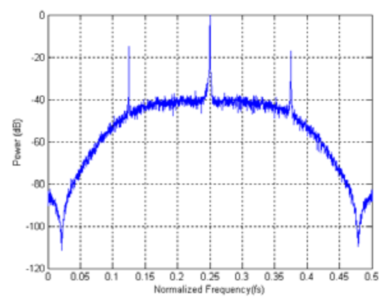

Fig.1. Power spectrum of the signal obtained by DCM scheme.

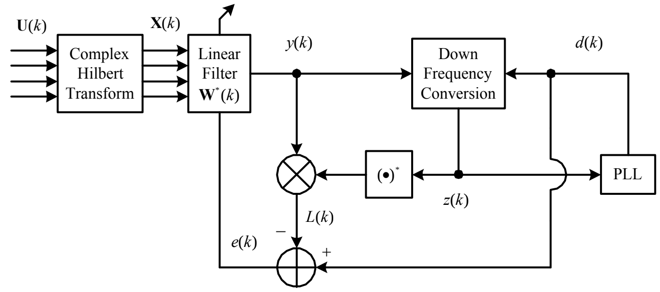

Fig.2. The structure of the blind adaptive beamformer

III. THE BLIND ADAPTIVE BEAMFORMER

The structure of the blind adaptive beamformer is proposed in Fig.2. Since the array output signal vector $\boldsymbol{U}(k)$ is bandpass (modulated) signal which is in the real form, the Hilbert transform is used to convert it into the complex form, i.e., $\boldsymbol{X}(k)=\boldsymbol{U}(k)+i\boldsymbol{U}(k)$, where $\boldsymbol{U}(k)$ is the Hilbert transform of $\mathbf{U}(k)$. As stated in section II, $L(k)$ contains a dominant peak at the carrier frequency f_c. Therefore, we propose to exploit the spectral line generation property by choosing the weights $\boldsymbol{W}$ of the hydrophone array in the derivations of adaptive bramforming to minimize the mean square error

$$J=\left\langle \left|d(k)-L(k)\right|^2\right\rangle \tag{3.1}$$

where $d(k)=e^{j2\pi f_c k}$ is the reference signal,

$$L(k)=y(k)y^*(k)d(k) \tag{3.2}$$

and the operator $\langle\bullet\rangle$ represents the time-averaging operation defined as

$$\langle\bullet\rangle \underline{\Delta} \lim_{T\to\infty}\frac{1}{T}\int_{-T/2}^{T/2}(\bullet)dt \tag{3.3}$$

Using the least-mean-square algorithm, the weight vector $\boldsymbol{W}(k)$ at time k is updated according to

$$\mathbf{W}(k+1)=\mathbf{W}(k)-\mu\nabla_{\mathbf{w}}J(k) \tag{3.4}$$

where μ is a step size in each iteration, and $\nabla_W J(k)$ represents the complex gradient of J with respect to $\boldsymbol{W}$ at each iteration k. 3.1) can be recast as

$$J(k)=e(k)e^*(k) \tag{3.5}$$

where $e(k) = d(k) - L(k)$. Because the weight values are complex, i.e.

$$w_i=a_i+jb_i \qquad i=1,2,\cdots \tag{3.6}$$

so, $\nabla_W J(k)$ may be calculated as follows:

$$\begin{aligned}\nabla_i J(k)&=\frac{\partial e(k)}{\partial a_i}e^*(k)+\frac{\partial e^*(k)}{\partial a_i}e(k)\\&+\frac{\partial e(k)}{\partial b_i}je^*(k)+\frac{\partial e^*(k)}{\partial b_i}je(k)\qquad ,i=1,\ 2,\cdots\end{aligned} \tag{3.7}$$

Replacing $e(k)$ with $d(k) - y(k)y^*(k)d(k)$ in 3.7), it follows that

$$\begin{aligned}\frac{\partial e(k)}{\partial a_i}&=-x_i(k)y^*(k)d(k)-x_i^*(k)y(k)d(k)\\\frac{\partial e(k)}{\partial b_i}&=jx_i(k)y^*(k)d(k)-jx_i^*(k)y(k)d(k)\\\frac{\partial e^*(k)}{\partial a_i}&=-x_i(k)y^*(k)d^*(k)-x_i^*(k)y(k)d^*(k)\\\frac{\partial e^*(k)}{\partial b_i}&=jx_i(k)y^*(k)d^*(k)-jx_i^*(k)y(k)d^*(k)\end{aligned} \tag{3.8}$$

where $x_i(k)$ is the received signal of the i-th sensor at time k. By substituting 3.8) into 3.7), we can get the complex gradient value of J for the i-th sensor as

$$\nabla_i J(k)=\text{-}2\left[x_i(k)y^*(k)d(k)e^*(k)+x_i(k)y^*(k)d^*(k)e(k)\right] \tag{3.9}$$

By substituting 3.9) into 3.4), we have the new weight vector updated according to

$$\begin{aligned}\boldsymbol{W}(k+1)&=\boldsymbol{W}(k)\\&+\mu_0\boldsymbol{X}(k)y^*(k)\left[d(k)e^*(k)+d^*(k)e(k)\right]\end{aligned} \tag{3.10}$$

where $0<\mu_0<(2/\lambda_{\max})$ and $\lambda_{\max}$ is the maximum eigenvalue of the array input signal's correlation matrix.

Finally, we summarize the relevant equations for the beamformer algorithm as follows:

$$\begin{aligned}y(k)&=\boldsymbol{W}^H(k)\boldsymbol{X}(k)\\z(k)&=y(k)d^*(k)\\L(k)&=y(k)z^*(k)\\e(k)&=d(k)-L(k)\\\boldsymbol{W}(k+1)&=\boldsymbol{W}(k)\\&+\mu_0\boldsymbol{X}(k)y^*(k)\left[d(k)e^*(k)+d^*(k)e(k)\right]\end{aligned} \tag{3.11}$$

IV. A SPACE-TIME PROCESSOR

The space-time processor has a cascading structure with BAB and DFE, shown in Fig.3. The DFE consists of a feed forward filter (FFF) and feedback filter (FBF) with joint coefficient vector $\boldsymbol{C}(k)$. Based on least-mean-square (LMS) or recursive least-square (RLS) algorithm, $\boldsymbol{C}(k)$ can be updated.

The algorithms of the space-time processor are listed as follows:

(1) BAB:

Using 3.11).

(2) DFE:

1. Based on LMS: (μ : step size)

$$I(k) = \boldsymbol{C}^H(k)\boldsymbol{z}(k)$$
$$\varepsilon(k) = D(k) - I(k) \text{ or } \hat{I}(k) - I(k)$$
$$\boldsymbol{C}(k+1) = \boldsymbol{C}(k) + \mu\varepsilon^*(k)\boldsymbol{z}(k)$$

2. Based on RLS: (λ : forgetting factor)

$$\boldsymbol{V}(k) = \Psi_\lambda^{-1}(k-1)\boldsymbol{z}(k)$$
$$\boldsymbol{K}(k) = \frac{\boldsymbol{V}(k)}{\lambda + \boldsymbol{z}^H(k)\boldsymbol{V}(k)}$$
$$I(k) = \boldsymbol{C}^H(k-1)\boldsymbol{z}(k)$$
$$\varepsilon(k) = D(k) - I(k) \text{ or } \hat{I}(k) - I(k)$$
$$\boldsymbol{C}(k) = \boldsymbol{C}(k-1) + \boldsymbol{K}(k)\varepsilon^*(k)$$
$$\Psi_\lambda^{-1}(k) = \lambda^{-1}\Psi_\lambda^{-1}(k-1) - \lambda^{-1}\boldsymbol{K}(k)\boldsymbol{z}^H(k)\Psi_\lambda^{-1}(k-1)$$

The space-time processor is aimed at suppressing interfering signals from directions out of the main beam and the ISI embedded in the symbol sequence. It has the salient features as follows: (1) the incident angle of the desired signal is not required, thus is robust against pointing error; (2) it is robust against the position error of the sensor array and avoids the cumbersome procedure of array calibration, since the steering vector is not used.

V. SIMULATION RESULTS

In the following computer simulation examples, the transmitted signal and the space-time processor are defined according to Table I and II, respectively. In Table I, we use QPSK as the modulation scheme. Before modulation, the message sequence has been shaped by the raised cosine filter with unity roll-off factor. The carrier frequency of QPSK modulated signal is 10 kHz. In Table II, we list all relevant parameters associated with the space-time processor.

In addition, a uniform linear array of four sensors with half wavelength of interelement spacing is used in BAB. The sampling rate is 40 kHz. The total amount of message bits is 2500. The received signal has $\pi/4$ phase shift relative to the transmitted signal.

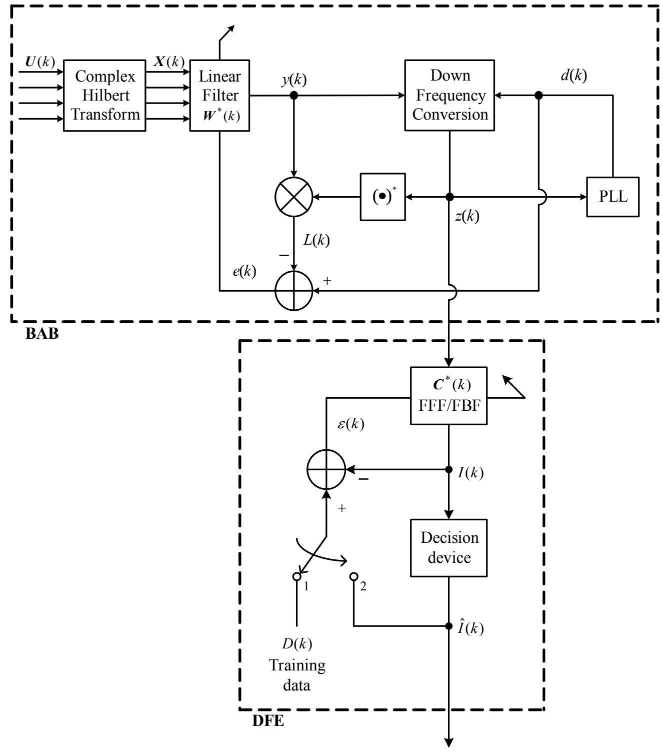

Fig.3. The structure of the space-time processor

In the first simulation example, performances of BAB, DFE and Space-Time (S-T) Processor are evaluated and compared for the case where one desired signal and two interference signals are present in additive white Gaussian noise. The desired and interference signals have different direction of arrival (azimuth), power and carrier frequency.

In real communication environment, interference may have various modulating formats. Thus, we adopt QPSK and AM as the modulation schemes for the interference signals. In AM, the modulation index is chosen to be 0.5 and the message frequency is 1 kHz. Table III lists the azimuths, powers and carrier frequencies of the desired and interference signals as well as the noise power.

In essence, the beamformer is a spatial filter and its purpose is to cancel interferences in spatial domain. Fig.4 shows the comparison of the transmitted desired baseband signals and the recovered baseband signals via BAB, DFE and S-T processor. For clarity of comparison, the transmitted desired baseband signal is also plotted in (b) ~ (f). We can clearly see that BAB, in (b), has a very good recovery of the transmitted desired signal and S-T processor, in (e) and (f), each has slightly better recovery than BAB alone. This indicates the DFE in S-T processor may be redundant in this type of channel.

But in (c) and (d), the DFE can not extract the desired signal by itself since it is only effective for combating ISI. If interference has different azimuth, DFE will fail to eliminate the interference.

Fig.5 is the diagram for signal constellations used as another tool for performance evaluation. As expected, it is compatible with the diagram shown in Fig.4. For symbol

Table I
Transmitted signal specification

Item	Specification
Modulation scheme	QPSK
Pulse shaping	Raised cosine filter (roll-off factor = 1)
Carrier frequency (f_c)	10k Hz

Table II
Space-time processor specification

BAB	
Item	Specification
Weight adaptation algorithm	LMS
Step-size (μ_0)	0.003
Initial weight vector	$[\,1\;0\;0\;0\,]^T$
DFE	
Item	Specification
Weight adaptation algorithm	LMS, RLS
Number of feedforward taps	13
Number of feedback taps	6
Step-size parameter of LMS	0.002
Forgetting factor of RLS	0.99
Initial weight vector of feedforward filter	[0…0 1 0…0]
Initial weight vector of feedback filter	[0…0]

Table III
Simulation conditions (1)

Signal	Azimuth	Power	Carrier frequency
QPSK (desired)	-10 degree	0 dB	10 kHz
QPSK	40 degree	-4 dB	8 KHz
AM	-40 degree	-4 dB	20 kHz
AWGN		-6 dB	

detection, BAB and S-T processor, in (b), (e) and (f), can do well but only DFE, in (c) and (d), fails. In (a), it is obtained by passing any one of the received signals through down-frequency converter representing the received (baseband) signal constellation. It is clear that the received signal is severely distorted by the channel.

Fig.6 shows the mean square errors (MSE) of DFE and S-T processor as a function of iteration number (samples). Because the S-T processor can operate correctly, the MSEs in (c) and (d) become stable after 1000 and 2000 samples

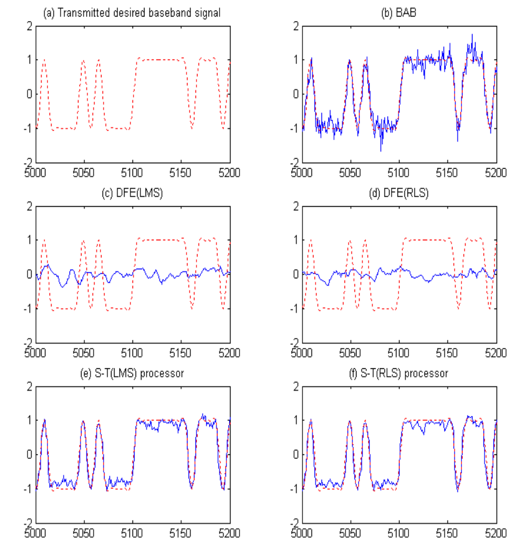

Fig.4. Baseband signal waveform (1).

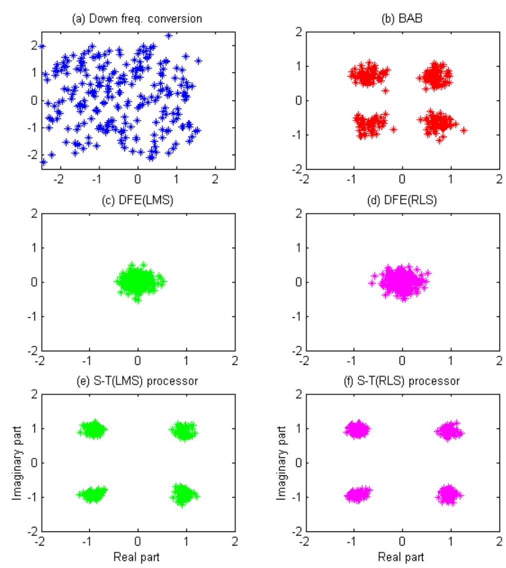

Fig.5. Signal constellation (1).

respectively. As expected, RLS has faster convergence than LMS. In (a) and (b), the MSEs fluctuate severely since the DFE fails to detect the correct symbols.

In the second simulation example, the multipath channel corresponds to multiple arrivals of coherent interference from different incident angles, resulting in severer ISI. Fig.7 shows the channel model where a_n is the attenuation factor, τ_n is the delay time of the n-th path and each path suffers from Rayleigh fading.

The simulation conditions used in the second simulation example are listed in Table IV In this case, there is no direct path (a_0=0) and each reflected path has different attenuation coefficient and symbol period of delay. Besides, the mobile

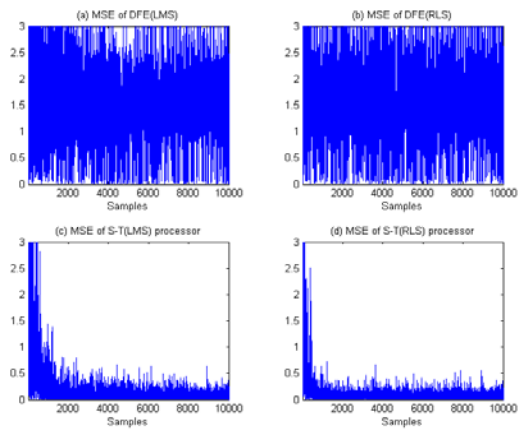

Fig.6. MSE performance (1).

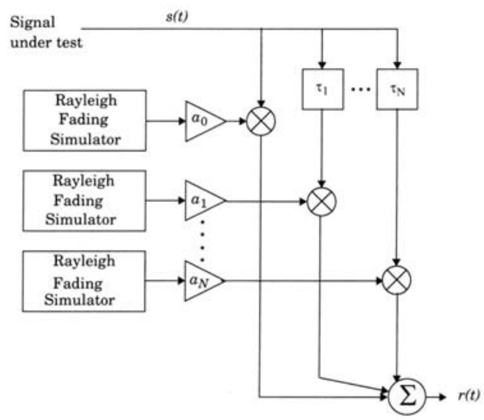

Fig.7. Multipath Rayleigh fading channel model.

Table IV
Simulation conditions (2)

Signal	Azimuth	Attenuation	Delay (symbol period)
Path1	0 degree	0.91	0.375
Path2	20 degree	0.83	0.625
Path3	-20 degree	0.77	1.125
Path4	-40 degree	0.62	1.625

speed is 10 km/hr, the transmitted signal power is 0 dB and AWGN power is -10 dB.

Fig.8 shows the waveforms of the transmitted and recovered signals using the BAB and the S-T processor. We can clearly see that the ISI effect from the multipath channel is more serious. The BAB can not combat the severe ISI but the S-T processor can.

Because the BAB output baseband signal is out of track, we expect that the signal constellation will not allow the BAB to discriminate the correct symbol. On the other hand, since the S-T processor can track the transmitted baseband signal quite well, its signal constellation will allow the processor to

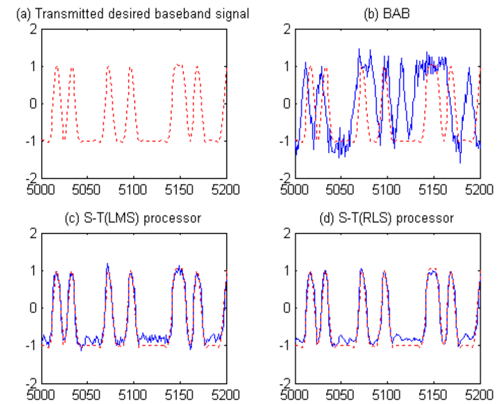

Fig.8. Baseband signal waveform (2)

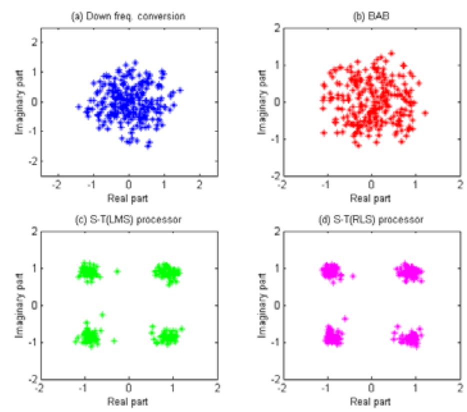

Fig.9. Signal constellation (2).

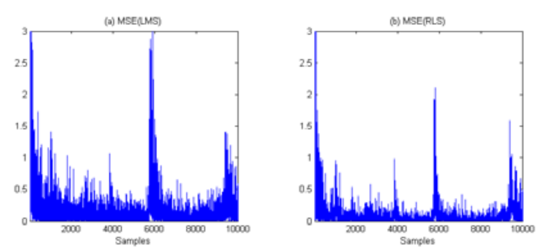

Fig.10. MSE of the S-T processor (2).

easily detect the correct symbol. This fact is demonstrated in Fig.9.

Fig.10 shows the MSE of the S-T processor, which is different from the previous ones. The weights of the S-T processor need to be retrained after certain amount of samples so as to adjust them to the channel variations. Again, RLS has faster convergence rate and smaller MSE than LMS.

In the third simulation example, the underwater acoustic (UWA) channel is at the location of 2 nautical miles short-range and 3.5 m depth shallow water [6]. The normalized impulse response, shown in Fig. 11, is used in the discrete-time ISI model.

This UWA channel has a temporal spread of 10 symbols

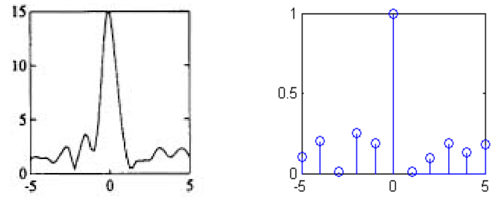

(a) (b)

Fig. 11. Underwater acoustic channel [6]: (a) channel impulse response (b) normalized discrete-time channel impulse response.

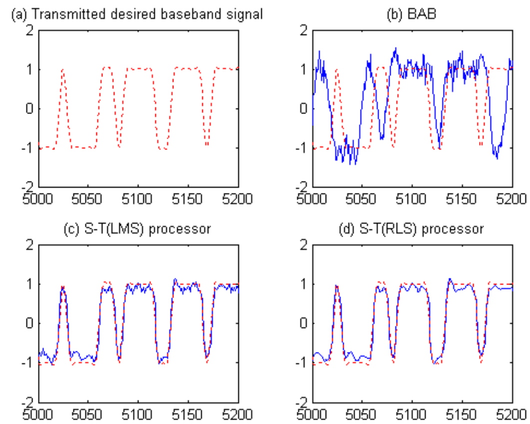

Fig.12. Baseband signal waveform (3).

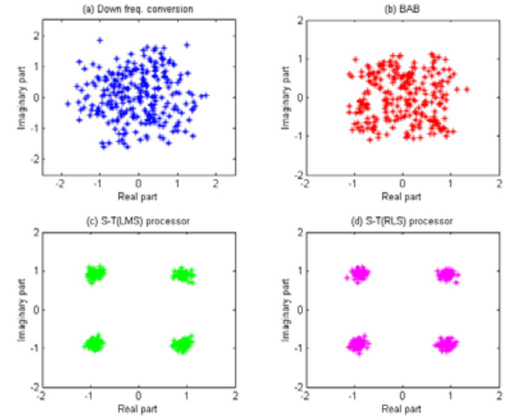

Fig.13. Signal constellation (3).

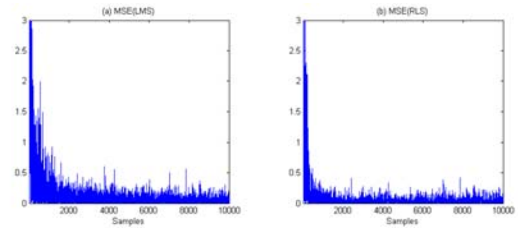

Fig.14. MSE of the S-T processor (3).

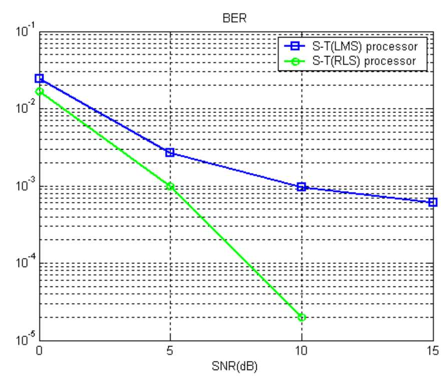

Fig.15. BER of the S-T processor for the underwater acoustic channel.

due to the ISI effect. The power of the transmitted signal is 0 dB and the azimuth of the received signal is -20 degree. Besides, we add a -6 dB white Gaussian noise.

The results of the recovered baseband signal in Fig.12 and signal constellation in Fig.13 show clearly that the BAB fails to eliminate the ISI effect, however, the S-T processor can recover the baseband signal and detect the original symbols very effectively.

The MSE of LMS- or RLS-based S-T processor in Fig. 14 shows that after some training data, both converge to a low and stable value. The convergence rate of RLS algorithm is faster than LMS algorithm.

In order to evaluate the bit error (BER), fifty thousand bits where transmitted over the underwater acoustic channel. Fig. 15 gives a plot of BER as a function of SNR for the S-T processor. It shows that the BERs for the S-T(LMS) and S-T(RLS) processors have descending trends as SNR increases. The S-T(RLS) processor has much faster descending rate of BER than the S-T(LMS) processor uniformly across the SNR range of 0~15 dB.

VI. CONCLUSIONS

We have devised a space-time processor which incorporates the blind adaptive beamformer with the adaptive decision feedback equalizer for phase-coherent digital wireless communication. The weight parameters of the blind adaptive beamformer are adaptively adjusted using a combination of the LMS algorithm and second-order digital PLL. The tap parameters of the equalizer are also adaptively adjusted by LMS and RLS algorithms, respectively.

We have adopted several types of channel model including multi-interference, Rayleigh multipath fading and UWA channels in computer simulations to evaluate the performances of BAB, DFE and the space-time processor. Simulation results include baseband signal diagrams, signal constellation diagrams and MSE curves. They all show that only the space-time processor can effectively recover the transmitted baseband signal and detect its symbol for all aforementioned type of channel model. The beamformer by itself can not combat ISI effect but can effectively eliminate interference signals with incident angles out of the main beam. On the contrary, the decision feedback equalizer by itself can't eliminate interferences in spatial domain but can effectively combat ISI effect. Therefore, the space-time processor is a powerful device for wireless communications.

In the future, we can exploit faster adaptive algorithms like RLS or Inverse QR Decomposition (IQRD) to substitute for the LMS algorithm in the blind adaptive beamformer. Blind characteristic can also be exploited for the adaptive decision feedback equalizer to eliminate the training periods or sequences. These features will facilitate real-time communication if provided.

Acknowledgements

This work was funded by the National Science Council in Taiwan. The authors gratefully thank it for the financial support.

References

[1] N. K. Jablon, "Adaptive beamforming with the generalized sidelobe canceller in the presence of array imperfections," *IEEE Trans. Antenna Propagat.*, vol. AP-34, pp. 996-1012, Aug. 1986.

[2] Luis Castedo and Anibal R. Figueiras-Vidal, "An adaptive beamforming technique based on cyclostationary signal properties," *IEEE Trans. Signal Processing*, vol. 43, pp. 1637-4650, July 1995.

[3] B. G. Agee, S. V. Schell, and W.A Gardner, "Spectral self-coherence restoral: A new approach to blind adaptive signal extraction using antenna arrays," *Proc. IEEE*, vol. 78, pp. 753-767, Apr. 1990.

[4] R. Gooch and J. Lundell, "The CM array: An adaptive beamformer for constant modulus signals," *Proc. ICASSP* '86, Tokyo, Japan, Apr. 1986, pp.2523-2526.

[5] Luis Castedo, Ching-Yih Tseng and Lloyd J. Griffiths, "A new cost function for adaptive beamforming using cyclostationary signal properties," *Proc. ICASSP* '94, Adelaide, Australia, vol. IV, pp. 249-252, Apr. 1994.

[6] M. Stojanovic, J. A. Catipovic, and J. G. Proakis, "Phase-coherent digital communications for underwater acoustic channels," *IEEE Journal of Oceanic Engineering*, vol. 19, pp. 100-111, Jan. 1994.